ACS Macro Letters

Letter

pubs.acs.org/macroletters

Free Energy of Defects in Ordered Assemblies of Block Copolymer Domains

Umang Nagpal,[†] Marcus Müller,[‡] Paul F. Nealey,[†] and Juan J. de Pablo*,[†]

[†]Department of Chemical and Biological Engineering, University of Wisconsin-Madison, Madison, Wisconsin 53706, United States

[‡]Institute for Theoretical Physics, Georg-August-Universität, 37077, Göttingen, Germany

Supporting Information

ABSTRACT: We investigate commonly occurring defects in block copolymer thin films assembled on chemically nanopatterned substrates and predict their probability of occurrence by computing their free energies. A theoretically informed 3D coarse grain model is used to describe the system. These defects become increasingly unstable as the strength of interactions between the copolymer and the patterned substrate increases and when partial defects occur close to the top surface of the film. The results presented here reveal an extraordinarily large thermodynamic driving force for the elimination of defects. When the characteristics of the substrate are commensurate with the morphology of the block copolymer, the probability of creating a defect is extremely small and well below the specifications of the semiconductor industry for fabrication of features having characteristic dimensions on the scale of tens of nanometers. We also investigate how the occurrence of defect changes when imperfections arise in the underlying patterns and find that, while defects continue to be remarkably unstable, stretched patterns are more permissive than compressed patterns.

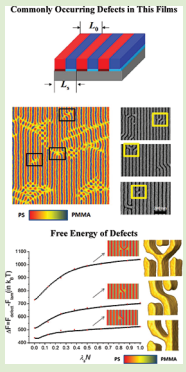

Block copolymers (BCPs) can self-assemble into complex morphologies, whose structure depends on the characteristics of the blocks. Their ability to self-assemble has led to applications ranging from thermoplastic elastomers to foams and adhesives. More recently, BCPs have received increased attention in the context of nanoscale fabrication, where the objective is to mass-produce precisely ordered nanoscale structures in the 3−50 nm range.[1,2] In a process referred to as BCP lithography,[2] a BCP film is used as a mask for subsequent etching of the underlying substrate. Several strategies have been pursued to achieve long-range order of the BCP mask. These include the application of shear, electric fields and the use of substrates having a chemical or a topographic pattern.[3−6] For applications in the semiconductor industry, it is essential to create BCP thin films that not only exhibit long-range order but also are free of defects over macroscopic areas in excess of 100 cm^2.[7] From an experimental point of view, finding a handful of nanometer scale defects in such large areas can be particularly demanding. We therefore turn to molecular models and statistical mechanical formalisms to determine the probability that distinct defects will arise in ordered BCP thin films.

Recent work has shown that directed self-assembly (DSA) of diblock copolymer films on chemically patterned substrates can be used to form regular structures (e.g., arrays of lines or dots) and irregular structures (e.g., bends or T-junctions).[8] Perhaps more importantly, DSA on chemical patterns appears to be particularly tolerant to imperfections of the underlying chemical pattern.[9,10] In this work we estimate the free energy of commonly observed BCP defects on stripe-patterned substrates, and we use those estimates to predict the probability that such defects will be observed over macroscopic areas of relevance to applications. To the best of our knowledge, the calculations reported here represent the first free energy predictions for distinct defects in the presence of fluctuations on chemically patterned substrates. The results provide an essential piece of information that has been lacking from discussions of the viability and scalability of BCP assembly for technology applications, namely, the equilibrium probability that common defects will be observed over large areas.

Defects in BCP thin films assembled on chemically patterned substrates may originate from pattern imperfections or may be due to kinetic entrapment of imperfect morphologies on a perfect substrate.[7,8,10−12] Several studies have examined the structure and dynamics of defects of BCP thin films on homogeneous surfaces.[13−19] Structural evolution on chemically patterned surfaces, however, is significantly different from that observed on homogeneous substrates.[12] Welander et al., for example, have shown that annealing at elevated temperatures leads to the formation of defect-free structures in a matter of minutes.[20] That study was particularly relevant to applications in that it was carried out on stripe-patterned substrates and with lamellar morphologies that offer potential for device fabrication. A more recent report, using industrial equipment and conditions, has presented a statistical, industrial scale analysis of defects over larger areas than those originally considered by Welander et al. and suggests that it might indeed be possible to obtain defect-free ordered copolymer films over macroscopic areas (with zero dislocation or disclination defects).[21]

Received: January 6, 2012
Accepted: February 25, 2012
Published: March 7, 2012

   dx.doi.org/10.1021/mz200245s | *ACS Macro Lett.* 2012, 1, 418−422

As useful and informative as past studies have been, the central questions regarding commonly occurring defects in ordered assemblies of BCPs on patterned substrates remain unanswered. These questions include (i) their actual size, (ii) their free energy and the role of fluctuations on that free energy, (iii) their relative stability, and (iv) the role of substrate patterns on their formation. We use a coarse grain model[22] to address such questions on three commonly occurring localized defects that are frequently observed in both experiments and simulations of BCPs on stripe-patterned substrates, namely, jogs, +1/2 disclinations, and edge dislocations (see Figure 1).

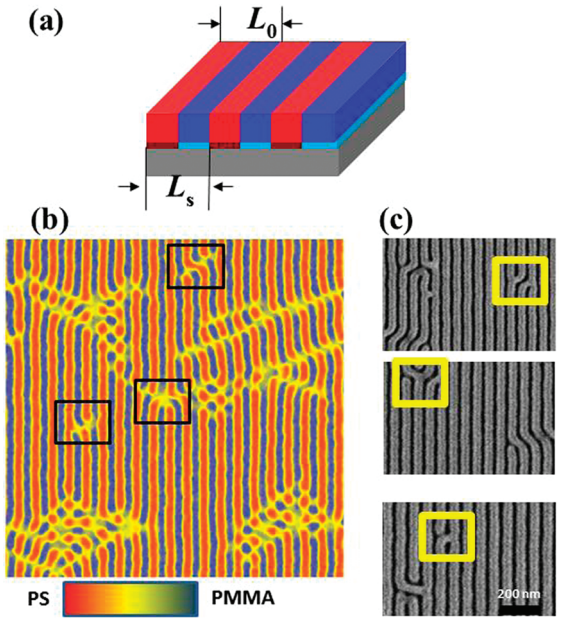

Figure 1. (a) Schematic representation of the simulated system: PS-*b*-PMMA with natural bulk morphological period L_0 assembled on a stripe-patterned substrate with periodicity L_s (= $1.0L_0$ in this case). Simulation (b) and experimental SEM (c) top-down views of ordered BCP copolymer thin films assembled on stripe-patterned substrates. The experimental images correspond to PS-*b*-PMMA with the molecular weight 176 kg/mol. The three short-range defects considered in this work are highlighted with black squares in the simulated image and with yellow squares in the experimental micrographs. The images on the right show a jog defect (top), a +1/2 disclination (middle), and an edge dislocation (bottom).

The model adopted in this work describes the copolymer system at the level of distinct macromolecules interacting with a fluctuating concentration field created by all of the other molecules in the system. That model is similar to that implemented in widely used self-consistent field theory descriptions of polymers and has been shown to be capable of describing quantitatively the structure and properties of thin BCP films assembled on patterned substrates.[22] The main properties that govern copolymer behavior at mesoscopic length scales are the interactions between monomers, quantified in terms of a Flory–Huggins parameter χ, a compressibility parameter given by κ, and a chain interdigitation parameter or invariant degree of polymerization denoted by $(\bar{N})^{1/2}$.[22] For the A–B diblock on chemically patterned stripes shown in Figure 1, we assume that, for both patterned areas, the repulsion for the nonpreferred block is equal in magnitude to the attraction for the preferred block ($\lambda_s^A N = -\lambda_s^B N$) where the parameter $\lambda_s N$ determines the strength of the interaction between the bead and the pattern. The simulation box has dimensions L_x, L_y, and L_z (thickness), respectively. A detailed description of the model is provided in the Supporting Information. Although the methodology presented in this work can be extended to polymers in the weak to strong segregation limit, the parameters employed in this work are representative of PS-*b*-PMMA (polystyrene-*b*-poly(methyl methacrylate)), specifically, symmetric chains of molecular weight 104 kg/mol with N = 32 beads.[22] Thermodynamic integration, as described in the Supporting Information, is used to compute the relative free energy of different structures.[11,23] Using this free energy, and using the expression $\exp(-\Delta F/k_B T)$, where ΔF is the free energy difference between two structures (k_B is the Boltzmann constant and T is temperature), one can find their relative probability of occurrence.

We begin by identifying the most common defects that arise in the DSA of symmetric diblock copolymer thin film lamellae on stripe-patterned substrates. Depending on annealing conditions, one can observe localized and spatially extended defects in both simulations and experiments. Figure 1 shows results from simulations of symmetric BCP film of thickness $1L_0 = 1.8R_e$ (where L_0 denotes the characteristic period of the lamellae in the bulk) and $\lambda_s N = 0.5$ following a step quench from a disordered state (corresponding to $\chi N = 0$) to an ordered state (corresponding to $\chi N = 37$). In the Supporting Information section we provide a detailed account of the sequence of morphologies that is observed during DSA. The stripes on the substrate have the period $L_s = L_0$. Figure 1 also shows experimental images for PS-*b*-PMMA with the molecular weight 176 kg/mol on a substrate having stripes of width L_s = 80 nm. One can see that the defects observed in experiments are qualitatively similar to those observed in simulations. A quantitative analysis of the dynamics and lifetime of defects is beyond the scope of the MC framework adopted in this work; here we merely note that a recent work has shown that the model adopted here provides a reasonable description of structural evolution in BCPs.[24] The images in Figure 1 serve to illustrate that the defects that occur with the highest frequency in simulated quenches are also observed with the highest probability in experiments after spin-coating and partial annealing. The defect configurations required for simulations of the free energy are generated as outlined above. Their free energy is determined relative to that of perfect lamellae assembled on the same substrates as the defects.

Figure 2 shows the free energy of the three defects considered here (simulation box $10L_0 \times 5L_0 \times 1L_0$) as a function of the interaction strength. Defect free energies are found to be on the order of several hundred $k_B T$. This order of magnitude can be rationalized by noting that the typical scale of the free energy of an interface between two differently oriented morphologies (grain boundary) scales as $k_B T\ ((\bar{N})^{1/2}/R_e^2)$ (where R_e is the mean squared end-to-end distance for an isolated noninteracting chain) and the cross section of the defect is on the order of $2L_sL_z$. Here we note that the defect free energies presented in Figure 2 have the reported order, 1/2 disclination > jog > edge dislocation; these energies correspond to 3, 2, and 1 broken lamellar lines, respectively. That ordering of free energies is also correlated with a decrease in the lateral size of the defects.

As $\lambda_s N$ increases, the free energy difference generally increases, confirming the view that defects become increasingly unstable as the strength of interactions between the copolymer and the pattern stripes increases. Two regimes can be identified

dx.doi.org/10.1021/mz200245s | ACS Macro Lett. 2012, 1, 418–422

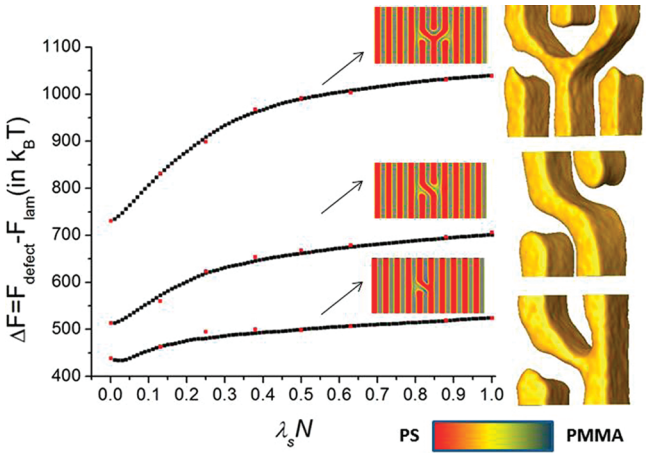

Figure 2. Free energy difference between defective and perfect lamellar structures as a function of interaction strength $\lambda_s N$ for three commonly occurring defects (+1/2 disclination on top, jog defect in the middle, and edge dislocation at the bottom). The three-dimensional PS domains (obtained at $\lambda_s N$ = 0.001) are shown on the right. The color map of simulation images appears on the bottom. The free energy was computed by two methods: thermodynamic integration (red dots for $\lambda_s N$ = 0.001, 0.13, 0.25, 0.38, 0.5, 0.63, 0.88, and 1.0), and simple thermodynamic integration (black line) along $\lambda_s N$, taking $\lambda_s N$ = 0.001 as the reference.

in the figure. For interaction strengths of $\lambda_s N < 0.01$, the defects are metastable; that is, they remain in place for protracted simulation times. Note that during thermodynamic integration, the ends of the integration paths are unconstrained; that is, the external field vanishes. The system is therefore allowed to explore all configurations that correspond to this metastable state, and thermodynamic integration along the reversible transformation path enables calculation of the corresponding free-energy difference. Additional details pertaining to the specific paths adopted here (and their corresponding contributions to the free energy) are provided in the Supporting Information section. The validity of the proposed approach was verified by computing the free energy using two different paths (see black symbols and red symbols in Figure 2), with identical results. One can observe a slight minimum in Figure 2, which is related to the transition between metastable defects, which go through to the substrate at small $\lambda_s N$, and unstable defects, at larger $\lambda_s N$, which exhibit an aligned ordered layer at the substrate. The formation of the aligned area reduces the excess free energy of the defect and leads to a weaker dependence of the excess free energy on the strength of the surface interactions. Thus for larger values of the stripe preference the defect structures are not even metastable; that is, a thin layer is first formed spontaneously, in which the BCP morphology is registered with the stripe pattern. The thickness of this registered layer gradually increases in time. For interaction strengths above 0.01 the free energy of the defects increases considerably. These results serve to rationalize experimental observations in which weakly preferential stripes are sufficient to prevent the metastability of defect structures.

To quantify the characteristic dimensions of a defect and its range of interaction with other defects, it is of interest to define its actual size in terms of the number of chains and its extension. We focus on the jog defect and perform simulations using different box sizes (we vary L_x and L_y while keeping L_z, the thickness of the film, equal to $1L_0$). We then compute the free energy difference for each box size relative to that of perfect lamellae of the same size. Our results, shown in Figure 3 for a value of $\lambda_s N$ = 0.5, indicate that the defect free energy

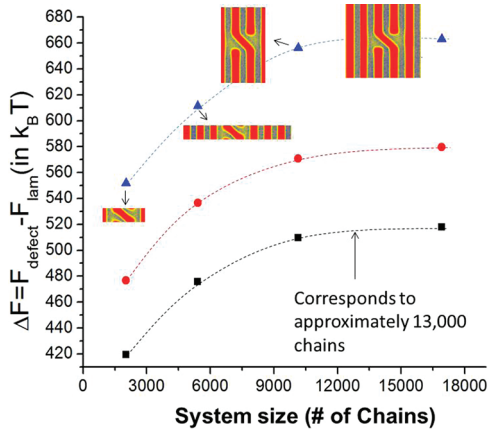

Figure 3. Free energy difference between a jog defect and perfect lamellae as a function of system size. The free energy was computed by thermodynamic integration for $\lambda_s N$ = 0.001, 0.13, and 0.5 shown as black squares, red circles, and blue triangles, respectively. Dotted lines are a fit to the points.

reaches an asymptotic, size-independent value when the number of molecules is approximately 13 000, corresponding to a box having dimensions $5L_0 \times 5L_0 \times 1L_0$. Beyond this system size, the total free energy difference is approximately 670 $k_B T$ (Figure 3) for $\lambda_s N$ = 0.5. Our simulations also reveal that the size of the defect is independent of the value of $\lambda_s N$.

Previous work has shown that in DSA on chemical patterns the BCP order grows from the substrate to the free surface.[12] During annealing, a defect will be healed from the bottom pattern to the top, in a process driven by the free energy of the remaining partial defect. An important concern that arises in practice is whether the underlying patterns themselves are perfect or not. It is therefore of interest to explore the stability of defects under suboptimal conditions, when the width of the pattern is smaller or larger than the characteristic period of the lamellae. In this work, for commensurate (L_s/L_0 = 1.0) and compressed lamellae (L_s/L_0 = 0.9), defect healing from the bottom surface is observed. However, for stretched lamellae structure (L_s/L_0 = 1.1), defect healing from both the bottom and the top surface is observed. To quantify the free energy of partial defects in commensurate, compressed and stretched lamellae, one can anneal a defective film for limited amounts of time, until distinct partial defects are observed. The free energy is then determined using the same procedure as that used for full defects. Since those partial defects are not even metastable, however, their free energy will depend on the manner in which the system is constrained. Thus removal of defects by increasing annealing time occurs spontaneously. Figure 4 shows the 3D PS domains of the partial defects studied in this work. One can see that defect removal occurs by increasing the thickness of the aligned defect-free layer at the substrate and thinning the thickness of the defect layer at the top of the film. Additional information is provided in the Supporting Information.

This mechanism of defect removal for commensurate and compressed lamellae is compatible with previous experiments.[12,20] More importantly, partial defects that occupy as little as a fifth of the film thickness (case V in Figure 4) continue to be remarkably unstable, with a free energy of nearly

dx.doi.org/10.1021/mz200245s | ACS Macro Lett. 2012, 1, 418−422

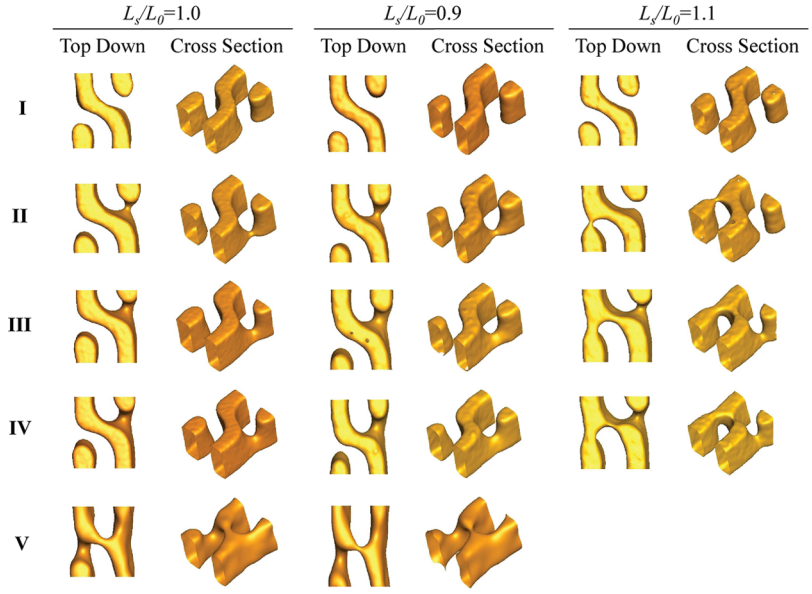

Figure 4. Three-dimensional representative configurations of PS domains (top down on left and cross section on right) corresponding to partial defects obtained at different annealing times for regular/stretched/compressed lamellae for L_s/L_0 = 1.0, L_s/L_0 = 0.9, and L_s/L_0 = 1.1, respectively. For L_s/L_0 = 1.0, the annealing times are 0, 10 000, 20 000, 30 000, and 40 000 MC steps for cases I to V, respectively. For L_s/L_0 = 0.9, the annealing times are 0, 40 000, 50 000, 60 000, and 70 000 MC steps for cases I to V, respectively. For L_s/L_0 = 1.1, the annealing times are 0, 30 000, 40 000, and 50 000 MC steps for cases I to IV, respectively, The defects were obtained for $\lambda_s N$ = 0.13.

300 k_BT. Using this value for the case of L_s/L_0 = 1.0, one can compute that, for an area of 100 cm^2, and using a defect size of $5L_0 \times 5L_0$, the probability of occurrence of a defect is 100 cm^2/defect size $\times$ exp($-\Delta F/k_BT$), which increases from 10^{-237} to 10^{-120} when the defect present at early annealing times (case I in Figure 4) evolves into a partial defect, as seen in case V in Figure 4. That is, the likelihood of forming a defect on commensurate stripe-patterned substrates is virtually nonexistent.

Of particular relevance is the fact that, by compressing the lamellae by 10%, the probability of a partial defect increases considerably. Specifically, for L_s/L_0 = 0.9 (images in Supporting Information), the probability of a defect can increase to 10^{-11}, much higher than that observed for commensurate stripes. In contrast, the probability of defect occurrence on stretched surface patterns is much lower than on compressed stripe patterns.

One of the remaining issues facing commercial fabrication of nanoscale patterns by DSA of copolymers on chemically patterned substrates is whether defect-free morphologies can indeed be produced over macroscopic areas. It can be argued that patterned substrates are "better" than nonpatterned substrates not because the equilibrium defect density is lower, but because patterns (i) direct the long-range structure[8,10] and (ii) they eliminate barriers toward defect removal by simple annealing. The latter is the focus in this work, where we have used a molecular model to demonstrate that, for lamellar structures, the free energy of defects is so large as to render the formation of common defects virtually impossible, even in situations when the underlying patterns are not commensurate with the characteristic dimensions of the lamellar morphology. Our results also indicate that erring on the side of stretched guiding patterns (as opposed to compressed patterns) in actual manufacturing processes is advantageous from a defect annealing perspective. For full or partial defects, the thermodynamic penalty associated with the formation of additional interfaces is overwhelming. Moreover, even very small preferences of the stripe pattern suffice to render defects completely unstable; that is, there is no barrier associated with their removal, but they are simply replaced by a registered morphology that is spontaneously formed at the patterned substrate and gradually grows thicker. Our results provide a fundamental explanation for recent, industrial-level empirical observations, which suggest that DSA on chemically patterned substrates may be capable of leading to perfect assemblies over commercially relevant, macroscopic domains. They also show that isolated defects are relatively small, thereby limiting their range of interaction. Strong interactions between the substrate and the copolymer destabilize defects and have the strongest impact at weak to intermediate values (in the vicinity of $0.02k_BT/nm^2$). While the study presented in this work has been limited to lamellar structures on striped substrates, it is precisely this type of morphology that is most relevant for applications of DSA in the context of magnetic storage media. Furthermore, the methods and formalism adopted in this work can be extended with little modification to other morphologies and have the potential to provide the basis for a priori, in silico evaluation of defect populations for specific designs.

■ ASSOCIATED CONTENT

Supporting Information

Further description and figures regarding the theoretically informed coarse grain model, thermodynamic integration, defect-free structur evolution, metastability of defect structures, the change in parameter ε with MC steps, and free energy difference as a function of parameter ε. This material is available free of charge via the Internet at http://pubs.acs.org.

■ AUTHOR INFORMATION

Corresponding Author

*E-mail: depablo@engr.wisc.edu.

Notes

The authors declare no competing financial interest.

■ ACKNOWLEDGMENTS

The authors are grateful for support from the Semiconductor Research Corporation (SRC) and the National Science Foundation (UW-NSEC, grant DMR-0832760). M.M. thanks the VW-Foundation for financial support.

■ REFERENCES

(1) Bates, F.; Fredrickson, G. *Phys. Today* **1999**, *52*, 32.
(2) Park, M.; Harrison, C.; Chaikin, P. M.; Register, R. A.; Adamson, D. H. *Science* **1997**, *276*, 1401.
(3) Lazzari, M.; Liu, G.; Lecommandoux, S. *Block Copolymers in Nanoscience*, Vol. *1*; Wiley-VCH: Weinheim, 2006.
(4) Park, S.; Lee, D. H.; Xu, J.; Kim, B.; Hong, S. W.; Jeong, U.; Xu, T.; Russell, T. P. *Science* **2009**, *323*, 1030.
(5) Bita, I.; Yang, J. K. W.; Jung, Y. S.; Ross, C. A.; Thomas, E. L.; Berggren, K. K. *Science* **2008**, *321*, 939.
(6) Darling, S. *Prog. Polym. Sci.* **2007**, *32*, 1152.
(7) Kim, S. O.; Solak, H. H.; Stoykovich, M. P.; Ferrier, N. J.; de Pablo, J. J.; Nealey, P. F. *Nature* **2003**, *424*, 411.
(8) Stoykovich, M.; Kang, H.; Daoulas, K. C.; Liu, G.; Liu, C.-C.; de Pablo, J. J.; Müller, M.; Nealey, P. F. *ACS Nano* **2007**, *1*, 168.
(9) Edwards, E.; Müller, M.; Stoykovich, M. P.; Solak, H. H.; de Pablo, J. J.; Nealey, P. F. *Macromolecules* **2007**, *40*, 90.
(10) Ruiz, R.; Kang, H.; Detcheverry, F. A.; Dobisz, E.; Kercher, D. S.; Albrecht, T. R.; de Pablo, J. J.; Nealey, P. F. *Science* **2008**, *321*, 936.
(11) Detcheverry, F.; Liu, G.; Nealey, P. F.; de Pablo, J. J. *Macromolecules* **2010**, *43*, 3446.
(12) Edwards, E. W.; Stoykovich, M. P.; Müller, M.; Solak, H. H.; de Pablo, J. J.; Nealey, P. F. *J. Polym. Sci., Part B: Polym. Phys.* **2005**, *43*, 3444.
(13) Hahm, J.; Lopes, W. A.; Jaeger, H. M.; Sibener, S. J. *J. Chem. Phys.* **1998**, *109*, 10111.
(14) Harrison, C.; Cheng, Z.; Sethuraman, S.; Huse, D. A.; Chaikin, P. M.; Vega, D. A.; Sebastian, J. M.; Register, R. A.; Adamson, D. H. *Phys. Rev. E* **2002**, *66*, 011706.
(15) Harrison, C.; Adamson, D. H.; Cheng, Z.; Sebastian, J. M.; Sethuraman, S.; Huse, D. A.; Register, R. A.; Chaikin, P. M. *Science* **2000**, *290*, 1558.
(16) Segalman, R.; Schaefer, K. E.; Fredrickson, G. H.; Kramer, E. J. *Macromolecules* **2003**, *36*, 4498.
(17) Tsarkova, L.; Horvat, A.; Krausch, G.; Zvelindovsky, A. V.; Sevink, G. J. A.; Magerle, R. *Langmuir* **2006**, *22*, 8089. Tsarkova, L.; Knoll, A.; Magerle, R. *Nano Lett.* **2006**, *6*, 1574.
(18) Horvat, A.; Sevink, G. J. A.; Zvelindovsky, A. V.; Krekhov, A.; Tsarkova, L. *ACS Nano* **2008**, *2*, 1143.
(19) Bosse, A. W.; Sides, S. W.; Katsov, K.; García-Cervera, C. J.; Fredrickson, G. H. *J. Polym. Sci., Part B: Polym. Phys.* **2006**, *44*, 2495.
(20) Welander, A.; Kang, H.; Stuen, K. O.; Solak, H. H.; Müller, M.; de Pablo, J. J.; Nealey, P. F. *Macromolecules* **2008**, *41*, 2759.
(21) Bencher, C.; et al. *Proc. SPIE* **2011**, *7970*, 79700F.
(22) Detcheverry, F.; Pike, D. Q.; Nagpal, U.; Nealey, P. F.; de Pablo, J. J. *Soft Matter* **2009**, *5*, 4858.
(23) Müller, M.; Daoulas, K. *J. Chem. Phys.* **2008**, *128*, 024903. Müller, M.; Daoulas, K.; Norizoe, Y. *Phys. Chem. Chem. Phys.* **2009**, *11*, 2087.
(24) Müller, M.; Daoulas, K. *J. Chem. Phys.* **2008**, *129*, 164906.